Nonlinear magnetoconductivity in Weyl and multi-Weyl semimetals in quantizing magnetic field

Sunit Das [*,†] Kamal Das [*,‡] and Amit Agarwal[§]

Department of Physics, Indian Institute of Technology, Kanpur-208016, India

Magnetotransport and magneto-optics experiments offer a very powerful probe for studying the physical properties of materials. Here, we investigate the second-order nonlinear magnetoconductivity of the tilted type-I Weyl and multi-Weyl semimetals. In contrast to the existence of chiral charge pumping in the linear response regime, we reproduce the absence of chiral charge pumping in the nonlinear transport regime, using the Boltzmann transport framework with the Landau levels. We predict that an inversion symmetry broken and tilted Weyl semimetal can support finite longitudinal nonlinear magnetoconductivity, which is otherwise absent in untilted Weyl semimetals. The nonlinear magnetoconductivity vanishes in the ultraquantum limit, oscillates in the intermediate magnetic field regime, and saturates in the semiclassical limit. The nonlinear magnetoconductivity depends intricately on the tilt orientation, and it can be used to determine the tilt orientation in Weyl and multi-Weyl semimetals, via nonlinear magnetoresistivity or second harmonic generation experiments.

I. INTRODUCTION

Since their discovery, Weyl semimetals (WSMs) have attracted significant attention due to their unusual linear quasiparticle dispersion mimicking the Weyl fermions with novel topological properties [1–6]. The combination of Weyl points in the bulk, which act as source and sink of Berry curvature with topological charges, and nontrivial Fermi arc surface states, support diverse novel transport and optical phenomena including the quantum anomalies [7–15]. Several of these phenomena have been experimentally realized in a wide range of materials showing Weyl characteristics, starting from the three-dimensional Dirac semimetal in the presence of a magnetic field [16,17] to transition metal mononictides [18–21] and magnetic materials [22–24]. Furthermore, the realization of WSMs in space inversion symmetry (SIS) broken systems has facilitated the exploration and potential application of second-order nonlinear (NL) responses [25–27]. It has been shown that the SIS broken WSMs exhibit photogalvanic responses [28–32] such as injection current [33] and shift current [34], second harmonic generation [35,36], sum and difference frequency generation [37], and the nonlinear Hall effect [38–40], among others.

Recently, there have been several studies focusing on how the NL transport and optical responses in WSMs are modified in the presence of a magnetic field. Treating the magnetic field within the semiclassical framework, it has been shown that the Berry curvature induces a finite NL magnetoconductivity [41–46]. In addition, the interband transition of carriers, combined with the chiral magnetic velocity gives rise to the helical

magnetic effect [47]. On the other hand, in the presence of a strong magnetic field where quantized Landau levels (LLs) are formed, optical transitions have been shown to generate photocurrent [30,48] in gyrotropic WSMs. More recently, second harmonic generation has been demonstrated in isotropic WSMs, in the presence of a DC electric field [49].

Motivated by these exciting studies, in this paper we explore the second-order NL magnetotransport/optical response in WSMs and in multi-WSMs [50–60] in the presence of a strong magnetic field that gives rise to discrete LLs [see Fig. 1(a)]. In order to treat the semiclassical, quantum oscillation, and the ultra-quantum transport regimes on the same footing, we apply the Boltzmann transport framework to the quantized LLs. Specifically, we calculate the intraband contribution to the NL longitudinal conductivity σ_{zzz}, which relates the second-order NL current to the applied electric fields, $j_z = \sigma_{zzz} E_z E_z$ [see Eq. (13)].

We consider a low energy model Hamiltonian describing a pair of tilted Weyl nodes of opposite chirality ($\chi = \pm 1$), specified by [61–63]

$$\mathcal{H}_\chi = \chi v_F \hbar \boldsymbol{k} \cdot \boldsymbol{\sigma} + \hbar \boldsymbol{w}_\chi \cdot \boldsymbol{k} \sigma_0. \tag{1}$$

Here, v_F is the Fermi velocity, $\boldsymbol{\sigma} = (\sigma_x, \sigma_y, \sigma_z)$ denotes the Pauli matrices, σ_0 is the identity matrix, and $\boldsymbol{w}_\chi$ represents the tilt velocity. We find that for having a finite NL longitudinal response, in addition to the broken SIS, the time-reversal symmetry (TRS) also needs to be broken. Different possible tilt orientations for the pair of opposite chirality Weyl nodes, and the resulting NL longitudinal conductivity are summarized in Fig. 1(b). We reproduce that WSMs do not support second-order NL chiral anomaly, i.e., there is no chiral charge pumping that is quadratic in electric field. Consequently, the whole NL longitudinal conductivity is determined by the intranode scattering times. We show that the NL longitudinal conductivity vanishes in the ultraquantum limit, indicating that the chiral LLs do not contribute to it. The NL conductivity

---

*These authors contributed equally to this work.

†sunitd@iitk.ac.in

‡kamaldas@iitk.ac.in
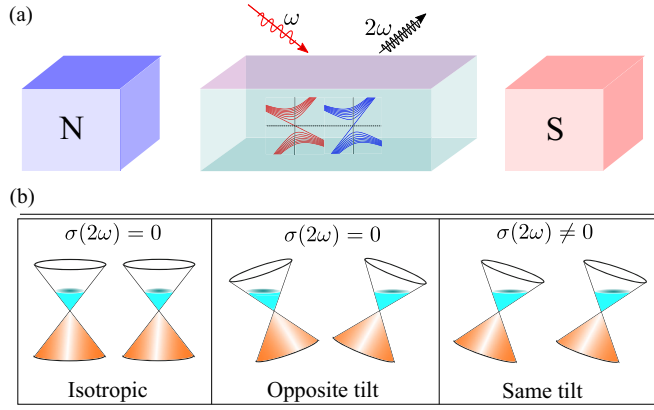
§amitag@iitk.ac.in

235408-1

FIG. 1. (a) A schematic of the second harmonic generation [$\sigma(2\omega)$] in the presence of a quantizing magnetic field. Panel (b) presents a summary of the various tilt orientations in WSMs, and the corresponding nonlinear responses. We show that the nonlinear longitudinal response is finite only when both the space inversion symmetry and time-reversal symmetry in WSMs are broken, with the tilt direction in the Weyl nodes of opposite chirality being aligned with each other.

shows an oscillating behavior in $1/B$ in the intermediate magnetic field regime, and the period of quantum oscillations can be used to measure the tilt velocity. In the semiclassical limit, the NL conductivity becomes independent of B reducing to the NL counterpart of the Drude conductivity. Our calculations reveal that these features of NL longitudinal response also persist in multi-WSMs.

II. SYMMETRIES AND TILT ORIENTATION IN WEYL SEMIMETAL

The TRS and SIS play a fundamental role in determining the low energy Hamiltonian of tilted WSMs [5,29,64,65], and consequently the NL responses. In space inversion symmetric (TRS broken) WSMs, minimum two nodes are feasible and the Weyl nodes of opposite chirality are related via the center of inversion [5]. In such systems, if the low energy model of one Weyl node in the Brillouin zone is given by $\mathcal{H} = \boldsymbol{\sigma} \cdot \boldsymbol{k} + \boldsymbol{w} \cdot \boldsymbol{k}$, then the Hamiltonian of the other node related through SIS is obtained by $\boldsymbol{k} \rightarrow -\boldsymbol{k}$ as $\mathcal{H}_{\mathcal{P}} = -\boldsymbol{\sigma} \cdot \boldsymbol{k} - \boldsymbol{w} \cdot \boldsymbol{k}$. This indicates that the SIS related Weyl nodes will always be oppositely tilted ($\boldsymbol{w}_- = -\boldsymbol{w}_+$). On the other hand, in a TRS preserving (SIS broken) WSM, a minimum of four nodes are needed. The Weyl nodes of the same chirality are related through a time-reversal invariant momentum while there is no symmetry restriction between the nodes with opposite chirality [5]. In this case, if the low energy model of one of the Weyl nodes is given by $\mathcal{H} = \boldsymbol{\sigma} \cdot \boldsymbol{k} + \boldsymbol{w} \cdot \boldsymbol{k}$, then the Hamiltonian of the other same chirality node related to it via TRS is obtained to be $\mathcal{H}_{\mathcal{T}} = \boldsymbol{\sigma} \cdot \boldsymbol{k} - \boldsymbol{w} \cdot \boldsymbol{k}$ [64]. This implies that nodes with the same chirality have opposite tilt. Since the second-order NL response vanishes in the presence of SIS, we consider the case of SIS broken WSMs, in which the Weyl nodes of opposite chirality have the same tilt velocity ($\boldsymbol{w}_+ = \boldsymbol{w}_-$). Within the family of SIS broken WSMs, we can consider systems either with TRS or without TRS. We show later that in TRS preserving WSMs, the longitudinal NL response vanishes [see

Eq. (15)]. Therefore, our work is focused on WSMs without any fundamental symmetries (both TRS and SIS are broken).

III. LANDAU LEVELS IN TILTED WEYL SEMIMETAL

The eigenvalue problem of massless tilted Dirac fermions in the presence of a strong magnetic field has been earlier explored in three-dimensional [64,66] systems as well as in two-dimensional [67,68] systems. Here, we sketch the calculation for a three-dimensional Weyl Hamiltonian given in Eq. (1). To be specific, we consider the magnetic field to be applied along the z axis ($\boldsymbol{B} = B\hat{z}$), and the tilt velocity to be in the x-z plane, $\boldsymbol{w}_\chi = (w_{\perp,\chi}, 0, w_{\parallel,\chi})$ having components parallel to and perpendicular to the applied magnetic field. We define the dimensionless quantities (i) $\boldsymbol{t}_\chi = \boldsymbol{w}_\chi/v_F = (t_{\perp,\chi}, 0, t_{\parallel,\chi}) = |\boldsymbol{t}_\chi|(\sin\theta, 0, \cos\theta)$, θ being the angle between the $\boldsymbol{w}_\chi$ and $\boldsymbol{B}$, and (ii) $\alpha = (1 - t_{\perp,\chi}^2)^{1/2}$, which will be used later. Depending on the dimensionless tilt strength, WSMs are categorized into two classes. For $|\boldsymbol{t}_\chi| < 1$, the Fermi surface of each Weyl node hosts only a closed electron or a closed hole pocket (in the absence of magnetic field) and such systems are called type-I WSMs. The systems with $|\boldsymbol{t}_\chi| > 1$ are called type-II WSMs, and in these systems the Fermi surface (in the absence of magnetic field) at the charge neutrality point consists of an open electron and an open hole pocket with the Weyl node connecting the two. In this paper, we focus on type-I WSMs.

To calculate the LLs, we use the Landau gauge to represent the magnetic field in the z direction via the vector potential $\boldsymbol{A} = (-By, 0, 0)$. In the presence of the vector potential, the Peierls substitution transforms the Hamiltonian as $\mathcal{H}_\chi = \chi v_F(\hbar\hat{\boldsymbol{k}} + e\boldsymbol{A}) \cdot \boldsymbol{\sigma} + \boldsymbol{w}_\chi \cdot (\hbar\hat{\boldsymbol{k}} + e\boldsymbol{A})\sigma_0$. The choice of the Landau gauge breaks the translational symmetry of the system along the y axis, but k_x and k_z remain good quantum numbers. Furthermore, the tilt in the Hamiltonian combined with the vector potential introduces a term like $-eyw_{\perp,\chi}B$, which can be seen as a potential resulting from an effective electric field $E_{\text{eff}} = w_{\perp,\chi}B$ along the negative y direction. Importantly, the LLs can exist only when the effective drift velocity $v_d = E_{\text{eff}}/B$ is less than the Fermi velocity, i.e., $w_{\perp,\chi} < v_F$ [69]. Now, introducing a Lorentz boost to eliminate the E_{eff} field, and after some little algebra we obtain the energy spectrum to be [64,66]

$$\epsilon_n^\chi = \begin{cases} (-\chi\alpha + t_{\parallel,\chi})\hbar v_F k_z & n = 0, \\ \text{sgn}(n)\alpha\mathcal{E}_{n,k_z} + \hbar v_F t_{\parallel,\chi} k_z & n \neq 0. \end{cases} \quad (2)$$

Here, we have defined $\omega_c = v_F/l_B$ with $l_B = \sqrt{\hbar/(eB)}$ and $\mathcal{E}_{n,k_z} = \sqrt{2|n|\alpha(\hbar\omega_c)^2 + (\hbar v_F k_z)^2}$. After Landau quantization, the three-dimensional problem effectively becomes a one-dimensional problem along the k_z axis. The LLs for a pair of Weyl nodes with opposite chirality and the same tilt velocity, are shown in Fig. 2. Some interesting facts about the LLs spectrum of tilted Weyl nodes are as follows: (i) For the lowest LL, the tilt only modifies the strength of the band velocity while for higher LLs the tilt introduces an additional term in the dispersion which is an odd function of k_z. We show below that the latter significantly modifies the NL conductivity. (ii) The tilt displaces the minima of the nonchiral LLs in the k_z axis and also squeezes their dispersion. The energy separation between consecutive LLs (at the minima) is given
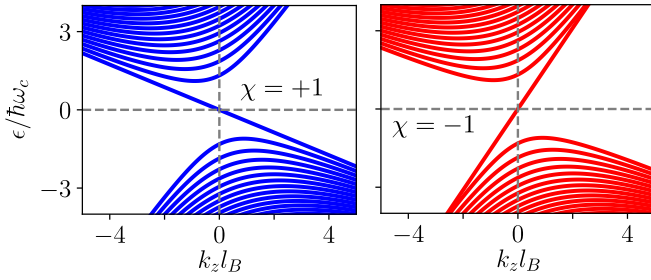
FIG. 2. Landau level spectrum of tilted type-I Weyl nodes with chirality $\chi = +1$ (left panel) and $\chi = -1$ (right panel). The energy axis is scaled with $\hbar\omega_c$ and the k_z axis is scaled with magnetic length l_B. The tilt has been considered to be oriented in the same direction for both Weyl nodes of opposite chirality. We have used $t_\chi = 0.6(\sin\theta, 0, \cos\theta)$ with $\theta = \pi/6$, Fermi velocity $v_F = 2 \times 10^5$ m/s, and magnetic field $B = 10$ Tesla.

by $\epsilon_{n+1} - \epsilon_n = [\alpha(1 - t_\chi^2)]^{1/2}\hbar\omega_c\sqrt{2(|n + 1| - |n|)}$, which is $[\alpha(1 - t_\chi^2)]^{1/2}$ times smaller than that in isotropic WSMs. (iii) The tilt removes the particle-hole symmetry which is otherwise present in isotropic Weyl nodes. (iv) The tilt does not alter the degeneracy of energy levels and it is the same as in isotropic WSMs, $\mathfrak{D} = 1/2\pi l_B^2$ per unit cross-section area perpendicular to the magnetic field [66].

It is straightforward to calculate the density of states, $\rho(\epsilon)$. For $\mu > 0$, we obtain $\rho(\epsilon)$ to be

$$\rho(\epsilon) = \rho_0\left[\frac{1}{\alpha - \chi t_{\parallel,\chi}} + \sum_{j=\pm,n=1}^{n_c}\left(\left|t_{\parallel,\chi} + \frac{\hbar v_F \alpha k_{z0}^j}{\mathcal{E}_{n,k_{z0}^j}}\right|\right)^{-1}\right]. \tag{3}$$

Here, we have defined $\rho_0 = 1/(4\pi^2 l_B^2\hbar v_F)$, and k_{z0}^j are the momentum points where the constant energy line (ϵ) intersects the LLs. The k_{z0}^j ($j = \pm$) are given by

$$k_{z0}^\pm(\epsilon) = \frac{\pm\sqrt{(1 - t_\chi^2)(k^2 - 2|n|\alpha^3/l_B^2) + k^2 t_{\parallel,\chi}^2} - kt_{\parallel,\chi}}{1 - t_\chi^2}, \tag{4}$$

with $k = \epsilon/\hbar v_F$. The density of states (DOS) in Eq. (3) is for the conduction band side ($\mu > 0$) and for more general form, we refer readers to Ref. [70]. For each of the LLs, the density of states diverges at $\epsilon_n = \sqrt{2|n|\alpha(1 - t_\chi^2)}\hbar\omega_c$. The group velocity along the z direction is calculated to be

$$v_{z,n}^\chi = \begin{cases} (-\chi\alpha + t_{\parallel,\chi})v_F & n = 0, \\ \text{sgn}(n)\alpha\hbar v_F^2 k_z/\mathcal{E}_{n,k_z} + v_F t_{\parallel,\chi} & n \neq 0. \end{cases} \tag{5}$$

The tilt introduces a constant velocity in each LL. The LL DOS and the group velocities will be used later to calculate the NL longitudinal conductivity.

IV. VANISHING NONLINEAR CHIRAL ANOMALY

It is well known in quantum field theories that there is no chiral charge pumping in the nonlinear transport regime [71]. Here, we reproduce this fact explicitly using the discrete LLs in combination with the Boltzmann transport framework. In the Boltzmann transport formalism, the current is calculated via the equation $j(t) = -e\mathfrak{D}\sum_{n,\chi}\int[dk_z]v_{z,n}^\chi f_n^\chi(t)$.

Here, "$-e$" denotes the electronic charge, $[dk_z] \equiv dk_z/(2\pi)$, and $f_n^\chi(t)$ is the nonequilibrium distribution function (NDF) in the presence of the applied external fields. To calculate the NL longitudinal conductivity, we consider a spatially uniform electric field oscillating at frequency ω and applied parallel to the magnetic field, $\boldsymbol{E}(t) = \hat{z}E_z e^{-i\omega t}$. In the linear response regime, the parallel electric and magnetic fields configuration (finite $\boldsymbol{E} \cdot \boldsymbol{B}$) induces chiral anomaly [7], the nonconservation of chiral charge in WSMs. The chiral charge pumping is countered by internode scattering to establish a steady state. Incorporating this in the Boltzmann equation, we can calculate the NDF [9].

Using the relaxation time approximation [11,66,72], we have

$$\partial_t f_n^\chi(t) + \dot{\boldsymbol{k}}_n^\chi \cdot \boldsymbol{\nabla}_k f_n^\chi(t) = -\frac{f_n^\chi(t) - \bar{f}_n^\chi(t)}{\tau} - \frac{\bar{f}_n^\chi(t) - f_n^0}{\tau_v}. \tag{6}$$

Here, $\bar{f}_n^\chi(t)$ represents the "local equilibrium" distribution function for each Weyl node. The global equilibrium distribution function is defined as $f_n^0 = [\bar{f}_n^\chi(t) + \bar{f}_n^{-\chi}(t)]/2$, which we assume to be the Fermi function, $f_n^0 = 1/[1 + e^{\beta(\epsilon_n^\chi - \mu)}]$ at chemical potential μ and inverse temperature $\beta = 1/(k_B T)$, with T and k_B being the temperature and the Boltzmann constant, respectively. The first term in the right-hand side of Eq. (6) represents the collision integral for the intranode scattering (with scattering rate $1/\tau$), which establishes the local equilibrium. The intranode scattering does not change the number of carriers in the respective node. The collision integral for internode scattering is represented by the second term in Eq. (6) with the internode scattering rate $1/\tau_v$. For simplicity, we ignore the energy dependence of both the scattering times. The NDF can be expressed as a sum of the equilibrium and nonequilibrium parts by expanding it in powers of the electric field strength, $f_n^\chi(t) = f_n^0 + f_n^{(1),\chi}e^{-i\omega t} + f_n^{(2),\chi}e^{-i2\omega t} + \cdots$. Here, $f_n^{(1),\chi}$ is linear order in the electric field, $f_n^{(2),\chi}$ is quadratic order in the electric field ($\propto |\boldsymbol{E}|^2$), and so on. In this paper, we are interested in the second-order response and hence we focus on calculating $f_n^{(2),\chi}$. The first question we address is the possibility of having NL chiral charge pumping in WSMs in which the rate change of chiral charge carriers will be proportional to $|\boldsymbol{E}|^2$.

To explore the NL chiral anomaly in WSMs, we start by reviewing the linear chiral anomaly and build the second-order response on top of that. The existence of linear chiral anomaly can be deduced from the collisionless Boltzmann equation [Eq. (6) with τ_v and $\tau \to \infty$], by using the equilibrium distribution function in the $\dot{\boldsymbol{k}} \cdot \boldsymbol{\nabla}_k f_n^\chi$ term and constructing a continuity equation [13,73]. Integrating over all the momentum states, we obtain [13]

$$\frac{\partial \mathcal{N}^{(1),\chi}}{\partial t} = -\mathfrak{D}\sum_n eE_z\int[dk_z]v_{n,z}^\chi(-\partial_\epsilon f_n^0)$$

$$= \frac{\chi e^2}{4\pi^2\hbar^2}E_z B. \tag{7}$$

Here, $\mathcal{N}^{(1),\chi} = \mathfrak{D}\sum_n\int[dk_z][f_n^{(0),\chi} + f_n^{(1),\chi}]$ is the particle number density in each Weyl node. Clearly, the chiral charge density is not conserved and this chiral charge pumping $\propto \boldsymbol{E} \cdot \boldsymbol{B}$ is the hallmark of linear chiral anomaly [9,13].

Using the same approach, we now verify for a NL version of the chiral anomaly by constructing a continuity equation with the NL distribution function. For the second-order NL chiral charge pumping equation, we need the first-order NDF. The first-order NDF can be calculated to be

$$f_n^{(1),\chi} = \left(-e\tau_\omega E_z v_{z,n}^\chi + \kappa \frac{\tau_\omega}{\tau_v} \langle \delta g_n^{(1),\chi} \rangle_\chi \right)(-\partial_\epsilon f_n^0). \quad (8)$$

Here, we have defined $\langle \delta g_n^{(1),\chi} \rangle_\chi = -e\tau_{v,\omega} E_z \langle v_{z,n}^\chi \rangle_\chi$, with $\langle \cdots \rangle_\chi = [\sum_n \int [dk_z](-\partial_\epsilon f_n^0)(\cdots)]/[\sum_n \int [dk_z](-\partial_\epsilon f_n^0)]$ denoting the average over all the electronic states at the Fermi level. Additionally, we have used $\tau_\omega = 1/(1-i\omega\tau)$, $\tau_{v,\omega} = 1/(1-i\omega\tau_v)$, and $\kappa = (\tau_v/\tau - 1)$. Integrating the collisionless Boltzmann transport equation over all the states in the DC limit ($\omega = 0$) we obtain

$$\frac{\partial \mathcal{N}^{(2),\chi}}{\partial t} = \frac{e^2 E_z^2 \tau}{4\pi^2 l_B^2} \left[(\mathcal{I}^\chi + \mathcal{C}_{22}^\chi) + \kappa \frac{\mathcal{C}_{11}^\chi}{\mathcal{C}_{01}^\chi} \mathcal{C}_{12}^\chi \right]. \quad (9)$$

Here, we have defined

$$\mathcal{I}^\chi = \sum_n \int dk_z \frac{\partial v_{z,n}^\chi}{\hbar \partial k_z}(\partial_\epsilon f_n^0), \quad (10a)$$

$$\mathcal{C}_{lm}^\chi = \sum_n \int dk_z (v_{z,n}^\chi)^l (\partial_\epsilon^m f_n^0). \quad (10b)$$

In the coefficient $\mathcal{C}_{lm}^\chi$, the first subscript denotes the power of the magnetic band velocity, and the second subscript denotes the order of the derivative of the Fermi function with respect to the energy. We find that $\mathcal{I}^\chi + \mathcal{C}_{22}^\chi = 0$, along with $\mathcal{C}_{12}^\chi = 0$, and consequently, $\partial \mathcal{N}^{(2),\chi}/\partial t = 0$. This reproduces the significant result that there is no NL chiral anomaly that is second order in the electric field strength. This is consistent with the absence of the nonlinear chiral anomaly in quantum field theories [71]. Thus, all chiral anomaly related NL transport phenomena in WSMs involve the linear chiral anomaly in combination with some other impact of the electric field.

V. NONLINEAR LONGITUDINAL CONDUCTIVITY

Having verified that the NL chiral anomaly vanishes, we show that the NL longitudinal conductivity is determined only by the intranode scattering contributions (see Appendix A for more details). The corresponding NDF is given by

$$f_n^{(2),\chi} = \frac{e^2 \tau_\omega \tau_{2\omega} E_z^2}{\hbar} \frac{\partial}{\partial k_z} \left[v_{z,n}^\chi (\partial_\epsilon f_n^0) \right], \quad (11)$$

where $\tau_{2\omega} = \tau/(1-i\tau 2\omega)$. Using the NDF in Eq. (11), the 2ω component of the longitudinal current density can be expressed as

$$j_z^{2\omega} = -e\mathfrak{D} \sum_{\chi=\pm 1, n=0}^{n=n_c} \int [dk_z] v_{z,n}^\chi f_n^{(2),\chi}. \quad (12)$$

Here, n_c is the number of filled (empty) LLs in the conduction (valence) band, and it is specified by $n_c = \text{int}[\frac{(\mu/\hbar\omega_c)^2}{2\alpha(1-t_\chi^2)}]$.

Evaluating Eq. (12) yields

$$\sigma_{zzz}(2\omega) = -\frac{e^3 \tau_\omega \tau_{2\omega}}{4\pi^2 \hbar^2 l_B^2} \sum_\chi \mathfrak{I}^\chi, \text{ where}$$

$$\mathfrak{I}^\chi = -\sum_n \int (\partial_{k_z} v_{z,n}^\chi)(\partial_{k_z} \epsilon_n^\chi) \partial_\epsilon f_n^0 dk_z. \quad (13)$$

In deriving Eq. (13), we have used $\int \hbar v_{z,n}^\chi \partial_{k_z} [v_{z,n}^\chi \partial_\epsilon f_n^0] dk_z = -\int (\partial_{k_z} v_{z,n}^\chi)(\partial_{k_z} \epsilon_n^\chi) \partial_\epsilon f_n^0 dk_z$. Using the LL spectrum in Eq. (13), we can now calculate the explicit form of the NL longitudinal conductivity, which is completely independent of the internode scattering timescale.

Clearly, the finite frequency NL conductivity is complex. The real part of the NL conductivity can be probed in nonlinear transport measurements. The imaginary part provides the information of second harmonic generation [74] where the NL optical susceptibility is given by $\chi_{zzz}(2\omega) = \sigma_{zzz}(2\omega)/(i2\omega\epsilon_0)$ [49] with ϵ_0 being the vacuum permittivity. Furthermore, the conductivity can be extracted in two different limits: (i) the transport (dominated by scattering) limit where $\omega\tau \ll 1$ and we get the transport conductivity proportional to τ^2 and independent of frequency, and (ii) the optical or clean limit $\omega\tau \gg 1$, where the NL optical conductivity is proportional to $1/\omega^2$ and independent of the scattering time.

A. Quantum oscillations in the nonlinear conductivity

In the presence of a strong magnetic field, the NL conductivity is expected to show quantum oscillation owing to the discrete LLs. To demonstrate this explicitly we calculate the contributions to the NL conductivity for each LL in the zero-temperature limit where the derivative of the Fermi function is approximated by the Dirac delta function. For the lowest LL ($n = 0$) we calculate

$$\mathfrak{I}^\chi = 0, \quad (14)$$

which implies that the chiral LL does not contribute to the longitudinal second-order NL response. This is in contrast to the linear response regime, where the chiral LLs have a finite contribution in the longitudinal conductivity [11,13,72]. However, this actually can be seen from Eq. (13). Since the velocity $v_{z,0}^\chi$ has no k_z dependence, the integrand of Eq. (13) itself is zero. The importance of this result can be appreciated from the fact that for a large enough magnetic field where only the lowest LL ($n = 0$) is filled, known as the ultraquantum limit, the NL longitudinal conductivity of the WSMs will vanish. More specifically, the ultraquantum regime is specified by $B > B_{\max} \equiv \frac{\mu^2}{2\hbar e v_F^2 \alpha(1-t_\chi^2)}$, and we predict that the NL longitudinal conductivity vanishes in this regime. This is also consistent with the vanishing NL chiral anomaly shown earlier.

The contributions from the higher LLs to the NL longitudinal conductivity, in the low-temperature limit (for $\mu > 0$) is given by

$$\mathfrak{I}^\chi = \sum_n \hbar v_F^2 2|n|(\alpha\hbar\omega_c)^2 \left[1/\mathcal{E}_{n,\tilde{k}_{z0}^+}^3 - 1/\mathcal{E}_{n,\tilde{k}_{z0}^-}^3 \right] n \geqslant 1. \quad (15)$$

Here, the momentum cuts $\tilde{k}_{z0}^\pm$ on the Fermi surface (μ) are obtained from Eq. (4) after substituting $k \to k_F = \mu/\hbar v_F$. We

note that Eq. (15) is independent of chirality and $\mathfrak{I}^\chi = 0$ for zero tilt ($t_{\parallel,\chi} = 0$). The latter can be seen from the fact that for zero tilt velocity, the momentum cuts on the Fermi surface satisfy $\tilde{k}_{z0}^+ = -\tilde{k}_{z0}^-$ and consequently $\mathcal{E}_{n,\tilde{k}_{z0}^+} = \mathcal{E}_{n,\tilde{k}_{z0}^-}$.

The result presented above is for a single Weyl node, and contributions from different Weyl nodes need to be added to obtain the total NL response. This is where the different symmetries of the WSMs, play a significant role in determining the total NL response from all Weyl nodes. We find that when $t_+ = -t_-$, the total NL conductivity, after summing over nodes of opposite chirality ($\mathfrak{I}^+ + \mathfrak{I}^-$), is identically zero. Using the explicit expression of $\mathcal{E}_{n,k_z}$ along with Eq. (4) in Eq. (15), we can simplify that $\mathfrak{I}^\chi \propto 1/(A - t_{\parallel,\chi})^{3/2} - 1/(A + t_{\parallel,\chi})^{3/2}$ where A is a quantity independent of the sign of tilt. It is clear from this simplified form that if we add contributions from opposite tilt, the total contribution becomes zero. This is also consistent with the fact that we have $t_+ = -t_-$ in WSMs with SIS [36,65]. Therefore, the total NL response is only nonzero when the Weyl nodes of opposite chirality have the same tilt orientation and in that case, the total contribution is double that of a single Weyl node. In a TRS invariant WSMs, a minimum of four nodes are allowed and the nodes with same chirality have opposite tilt orientation. In that case, since Eq. (15) is chirality independent, the total NL response from the same chirality nodes will be opposite to each other and the total response will be identically zero. Therefore, we conclude that the NL conductivity discussed in this paper is nonzero only in WSMs where both the TRS and the SIS are broken.

The oscillating nature of the NL conductivity as a function of the applied magnetic field is shown in Fig. 3(a). As expected the NL conductivity increases with the increase in tilt. Depending on the strength of the magnetic field, three key features can be inferred from the plot. In the small magnetic field (semiclassical) regime with a large number of filled LLs, the NL conductivity is almost independent of the magnetic field. In the ultraquantum regime for a large magnetic field, $B > B_{\max}$ to be precise, the NL conductivity vanishes. In the intermediate range of the magnetic field, we see a pronounced quantum oscillation feature. The usual periodic nature of the quantum oscillations in $1/B$ can be clearly seen in Fig. 3(b). We calculate the oscillation period to be

$$\Delta(1/B) = 2\alpha\left(1 - t_\chi^2\right)e\hbar(v_F/\mu)^2. \tag{16}$$

At its core, this period of quantum oscillations arises from the corresponding period in the density of states, and it manifests in linear as well as in NL magnetotransport. We show the chemical potential dependence of the NL conductivity in Fig. 4. For a fixed value of the magnetic field, we find quantum oscillation in the intermediate range of chemical potential and the NL conductivity vanishes for a small value of μ (ultraquantum regime). For a large value of μ, when several LLs are filled (semiclassical regime), the NL conductivity has a linear μ dependence. We emphasize here that the presence of a finite tilt velocity, breaks the particle-hole symmetry and consequently the NL conductivity of the valence band side ($\mu < 0$) is different from that in the conduction band side. The NL conductivity of the valence band side has the same form
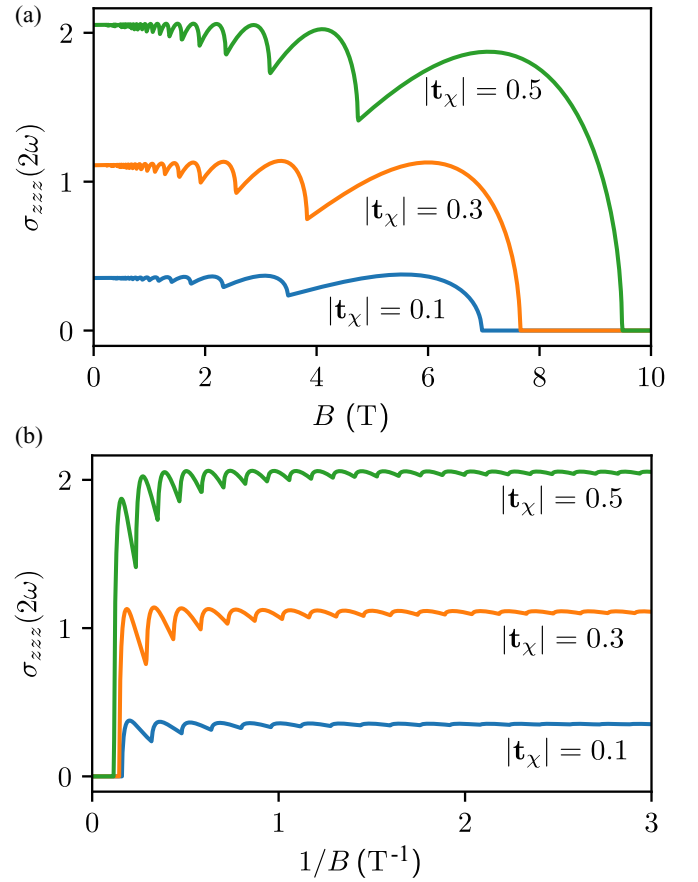

FIG. 3. The nonlinear conductivity of a pair of Weyl nodes as a function of (a) the magnetic field (B) and (b) the inverse of the magnetic field ($1/B$) for $\mu = 20$ meV. The conductivity axis has been scaled by $e^3 \tau_\omega \tau_{2\omega} \mu/\hbar^3 \times 10^{-2}$ and we have considered $t_\chi = -|t_\chi|(\sin\theta, 0, \cos\theta)$ with $\theta = \pi/6$. We note that both the plots complement each other. Clearly, the NL conductivity vanishes in the ultraquantum limit [right (left) side of the panel (a) [(b)]], and it becomes constant in the semiclassical regime.

as Eq. (15); however, the Fermi surface cuts are modified to

$$\tilde{k}_{z0}^{v,\pm} = \frac{k_F t_{\parallel,\chi} \pm \sqrt{\left(1 - t_\chi^2\right)\left(k_F^2 - 2|n|\alpha^3/l_B^2\right) + k_F^2 t_{\parallel,\chi}^2}}{\left(1 - t_\chi^2\right)}, \tag{17}$$

where $k_F = |\mu|/\hbar v_F$. Using this we can see that the NL conductivity has a different sign depending on whether μ is lying in the conduction band or in the valance band. This can be clearly seen in Fig. 4.

B. Semiclassical limit of the nonlinear conductivity

In the semiclassical limit where many LLs are filled, we can assume the LL index n to be a continuous variable and replace the $\sum_n$ by $\int_0^{n_c} dn$ in Eq. (13). Using this integration trick with appropriate limits, it is straightforward to calculate the semiclassical limit of Eq. (13). Unfortunately, it has quite a complicated form which obfuscates physical insights. However, the limiting case of small tilt velocity is more tractable, and offers useful insights. So we retain the tilt velocity in Eq. (15) only up to linear order, and then take
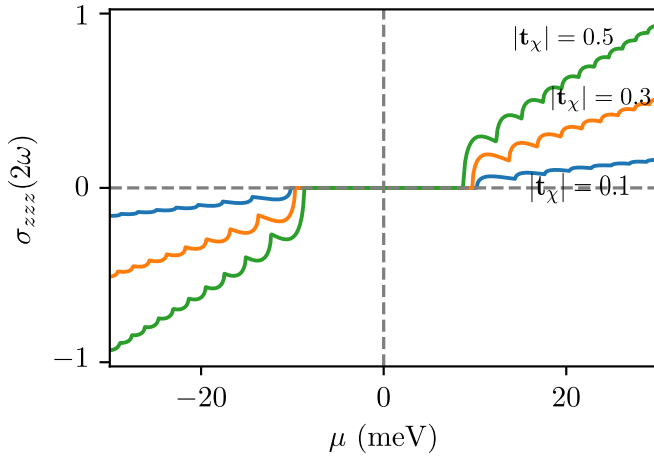
FIG. 4. The nonlinear conductivity of a pair of Weyl nodes as a function of chemical potential μ for $B = 2$ Tesla. The NL conductivity has been scaled by $e^3 \tau_\omega \tau_{2\omega}/(\hbar^2 \tau)$. We find that the NL conductivity has opposite sign for the chemical potential lying in the valence band and in the conduction band. While the tilt breaks the particle-hole symmetry, the difference between the magnitude of the NL conductivity in the conduction band and the valance band is not significant. The tilt parameter used here is the same as that in Fig. 2, and we have chosen $\tau = 10^{-12}$ s.

the semiclassical limit. Following this, we approximate $\tilde{k}_{z0}^{\pm} \approx \pm \sqrt{(k_F^2 - 2|n|/l_B^2)} - k_F t_{\parallel,\chi}$, and consequently $\mathcal{E}_{n,\tilde{k}_{z0}^{\pm}} \approx [\mu^2 \mp 2\mu t_{\parallel,\chi}\sqrt{\mu^2 - 2|n|(\hbar\omega_c)^2}]^{1/2}$. Using these simplifications, we find that $\mathfrak{J}^\chi$ in the small tilt velocity approximation is given by

$$\mathfrak{J}^\chi \approx \sum_n \hbar v_F^2 2|n|(\hbar\omega_c)^2 \frac{6 t_{\parallel,\chi}}{\mu^4} \sqrt{\mu^2 - 2|n|(\hbar\omega_c)^2}. \quad (18)$$

The approximate expression of the NL conductivity is obtained using Eq. (18) in Eq. (13). We find that the NL conductivity exhibits quantum oscillation behavior in $1/B$, due to the LL crossing the chemical potential [see the term $\sqrt{\mu^2 - 2|n|(\hbar\omega_c)^2}$ in Eq. (18)], with periodicity $\Delta(1/B) = 2e\hbar(v_F/\mu)^2$. This period is identical to that found in the linear magnetoconductance of a WSM without any tilt velocity [49]. Within the linear order tilt approximation, the maximum filled LL index is simplified as $n_c = \text{int}[\mu^2/2\hbar^2\omega_c^2]$.

Using these, it is straightforward to obtain $\mathfrak{J}_{\text{SC}}^\chi = \frac{4}{5\hbar} l_B^2 t_{\parallel,\chi} \mu$ in the semiclassical regime. Consequently, the semiclassical NL conductivity is given by

$$\sigma_{zzz}^{\text{SC}}(2\omega) = -\frac{e^3 \tau_\omega \tau_{2\omega}}{\pi^2 \hbar^3} \frac{\mu}{5} \sum_\chi t_{\parallel,\chi}. \quad (19)$$

We find that the NL conductivity in the semiclassical regime is (i) B independent, and (ii) it varies linearly with μ. The first observation is quite remarkable, and this is also consistent with the more general plot of Fig. 3. To understand this better, let us take the extreme limit of zero magnetic fields. In the $B \to 0$ limit, the longitudinal NL conductivity should be identical to the NL Drude conductivity, specified by $\sigma_{zzz}(2\omega) = -e^3 \tau_\omega \tau_{2\omega}/\hbar \sum_\chi \int [dk] v_z \partial_{k_z}(v_z f')$ [38,75]. Evaluating this expression, we find that it is identical to the

magnetoconductivity obtained in Eq. (19), establishing the consistency of our calculations. Since the NL Drude conductivity can only be finite in materials in which both the TRS and SIS are broken, this also helps in understanding the symmetry imposition (absence of both TRS and SIS) for having a finite NL longitudinal magnetoconductivity in tilted WSMs.

VI. NONLINEAR CONDUCTIVITY IN MULTI-WEYL SEMIMETAL

Having demonstrated longitudinal NL magnetoconductivity in tilted WSMs, we now show their presence in multi-WSM [52,53]. The multi-WSMs possesses nodes with chirality that have a nonzero integer value. The WSMs can be considered to be a special case with the chirality of ± 1. The low energy model Hamiltonian of multi-WSMs is given by [54,55]

$$\mathcal{H}_\chi^\nu = \chi[\alpha_\nu(\hbar k_\perp)^\nu \{\cos(\nu\phi)\sigma_x + \sin(\nu\phi)\sigma_y\} + \hbar v k_z \sigma_z] + \hbar \boldsymbol{w}_\chi \cdot \boldsymbol{k} \sigma_0. \quad (20)$$

Here, $k_\perp = \sqrt{k_x^2 + k_y^2}$ is the perpendicular momentum, $\tan\phi = k_y/k_x$, ν denotes the chiral charge, and α_ν is a material-dependent parameter. The LL problem of a system described by Eq. (20) in the absence of tilt ($\boldsymbol{w}_\chi = 0$) has been earlier explored in Refs. [50,51]. Here, we generalize the LL spectrum for the tilted type-I multi-WSMs (see Appendix B for details). For simplicity, we assume that the tilt is parallel to $\boldsymbol{B}$, i.e., $\boldsymbol{w}_\chi = (0, 0, w_{\parallel,\chi}) = v(0, 0, t_{\parallel,\chi})$. We find the LL spectrums to be

$$\epsilon_n^\chi = \begin{cases} -\chi\hbar v k_z + \hbar w_{\parallel,\chi} k_z & \text{for } n < \nu, \\ s\sqrt{\mathcal{F}(n, \alpha_\nu, B) + \epsilon_z^2} + \hbar w_{\parallel,\chi} k_z & \text{for } n \geqslant \nu. \end{cases} \quad (21)$$

Here, we have defined $\mathcal{F}(n, \alpha_\nu, B) = n(n-1)\ldots(n - \nu + 1)\omega_\nu^2$, $\omega_\nu = \alpha_\nu(\sqrt{2}\hbar/l_B)^\nu$, $\epsilon_z = \hbar v k_z$, and $s = \pm$ where $+ (-)$ represents the energy for the conduction (valence) band side. The lowest LLs are chiral, disperse linearly, and they are ν-fold degenerate.

The NL conductivity in the quantum oscillation regime in multi-WSMs has the same form as Eq. (13), with the modified $\mathfrak{J}^\chi$ specified by

$$\mathfrak{J}^\chi = \sum_n \hbar v^2 \mathcal{F}(n, \alpha_\nu, B) \left[1/\mathcal{E}_{n,\tilde{k}_{z0}^+}^3 - 1/\mathcal{E}_{n,\tilde{k}_{z0}^-}^3 \right], \quad n \geqslant \nu. \quad (22)$$

Here, $\mathcal{E}_{n,\tilde{k}_{z0}} = [\mathcal{F}(n, \alpha_\nu, B) + (\hbar v \tilde{k}_{z0})^2]^{1/2}$. The momentum corresponding to the Fermi surface is specified by

$$\tilde{k}_{z0}^\pm = \left[\pm \sqrt{(1 - t_{\parallel,\chi}^2)[k_F^2 - \mathcal{F}(n, \alpha_\nu, B)/(\hbar v)^2] + k_F^2 t_{\parallel,\chi}^2} - k_F t_{\parallel,\chi} \right](1 - t_{\parallel,\chi}^2)^{-1}. \quad (23)$$

Here, we have used $k_F = \mu/(\hbar v)$. To calculate the total NL current, we sum over all the occupied nondegenerate ($n \geqslant \nu$) LLs in Eq. (13) where the maximum filled LL index n_c is specified by $\mathcal{F}(n, \alpha_\nu, B) = \mu^2/(1 - t_{\parallel,\chi}^2)$. We have shown the oscillating NL conductivity of a double WSMs in Fig. 5 as a function of the magnetic field with $n_c = \text{int}[1/2 + \sqrt{1/4 + \mu^2/[\omega_2^2(1 - t_{\parallel,\chi}^2)]}]$. We find that the multi-WSMs shows features in the NL conductivity, which are very similar
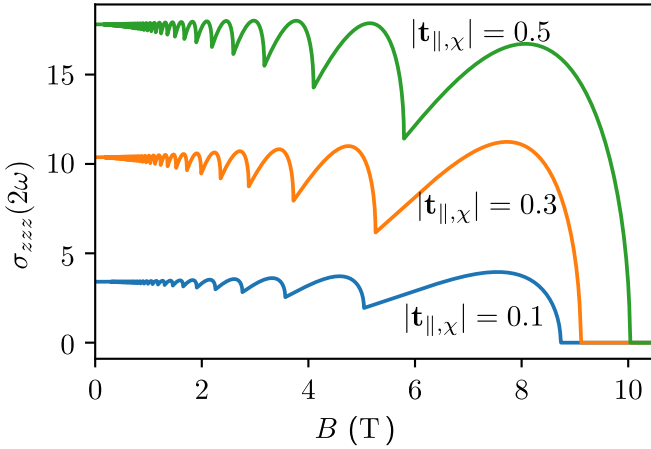
FIG. 5. The nonlinear conductivity of a double Weyl node as a function of the magnetic field $\boldsymbol{B}$ for $\mu = 0.15$ meV. The NL conductivity axis has been scaled by $e^3 \tau_\omega \tau_{2\omega} \mu / \hbar^3$ and we have considered $\boldsymbol{t}_\chi = -|\boldsymbol{t}_{\parallel,\chi}|(0, 0, 1)$. Here, we have used $\alpha_2 = 0.4$ eV Å$/\hbar^2$ and $v = 0.37$ eV Å$/\hbar$ [55].

to those calculated for WSMs. Specifically, we find that the NL conductivity vanishes in the ultraquantum limit, oscillates in the intermediate regime, and saturates in the semiclassical regime. Furthermore, the fundamental symmetry constraints and the relative tilt orientation of the multi-Weyl nodes of opposite chirality to get nonzero $\sigma_{zzz}(2\omega)$ in multi-WSMs are also the same as those in WSMs. However, we note that the double WSMs can withstand the oscillation in NL conductivity for a relatively large magnetic field value or very low chemical potential as compared to the WSMs.

VII. DISCUSSIONS AND CONCLUSION

To summarize, we have demonstrated the existence of finite NL longitudinal magnetoconductivity in type-I WSMs with quantized LLs. We show that the NL longitudinal conductivity is finite only in WSMs where both the TRS and SIS are broken. We demonstrate that the NL conductivity is solely determined by intranode scatterings and (i) vanishes in the ultraquantum limit where only the chiral LL are occupied, (ii) displays quantum oscillations in $1/B$ with a tilt velocity-dependent period, and (iii) becomes B independent in the semiclassical regime, reducing to the NL generalization of the Drude conductivity. Further analysis reveals that similar physics is also at play in the broader class of tilted multi-WSMs. The NL conductivity discussed in this paper will manifest through NL resistance in the case of transport experiments while through second harmonic generation in optical experiments. Due to the decisive dependence of the NL conductivity on the tilt orientation, we believe that our study will play a pivotal role in determining the tilt configuration of real Weyl materials.

Note added. Recently, we came across Ref. [76] by Zeng *et al.* where the nonlinear planar Hall effect is explored.

APPENDIX A: DERIVATION OF SECOND-ORDER NONEQUILIBRIUM DISTRIBUTION FUNCTION

In this Appendix, we provide the intermediate steps for calculating the second-order NDF. To calculate this, first we need the linear order distribution function. The latter has been calculated earlier in several references [11,66,72]. With an ansatz of the form $f_n^{(1),\chi} = \delta g_n^{(1),\chi}(-\partial_\epsilon f_n^0)$, the Boltzmann equation up to linear order in electric field can be constructed as

$$-i\omega \delta g_n^{(1),\chi} - eE_z v_{z,n}^\chi = -\frac{\delta g_n^{(1),\chi} - \delta \bar{g}_n^{(1),\chi}}{\tau} - \frac{\delta \bar{g}_n^{(1),\chi}}{\tau_v}. \quad (A1)$$

Using the particle number conservation within each node, it is straightforward to calculate the linear distribution function which is given in Eq. (8) of the main text. To calculate the second-order NDF, we extend the same formalism to include the quadratic electric field effects. Since the second-order NDF is expected to contain both the first and second derivative of the Fermi function, we consider an ansatz of the form

$$f_n^{(2),\chi} = \delta g_n^{(21),\chi}(-\partial_\epsilon f_n^0) + \delta g_n^{(22),\chi}(-\partial_\epsilon^2 f_n^0). \quad (A2)$$

Here, the first superscript (i) in $\delta g_n^{(ij),\chi}$ denotes the electric field dependence and the second superscript (j) denotes the order of energy derivative on the Fermi function. To begin with, we consider that the second-order distribution function changes the local equilibrium and the local part has the following form:

$$\bar{f}_n^{(2),\chi} = \delta \bar{g}_n^{(21),\chi}(-\partial_\epsilon f_n^0) + \delta \bar{\bar{g}}_n^{(22),\chi}(-\partial_\epsilon^2 f_n^0). \quad (A3)$$

Here, $\delta \bar{g}_n^{(21),\chi} \equiv \langle \delta g_n^{(21),\chi} \rangle_\chi$, and the definition of average is the same as defined in the main text. However, for the $\delta \bar{\bar{g}}_n^{(22),\chi} \equiv \langle\langle \delta g_n^{(22),\chi} \rangle\rangle_\chi$ we define

$$\langle\langle \cdots \rangle\rangle_\chi = \frac{\sum_n \int [dk_z](-\partial_\epsilon^2 f_n^0)(\cdots)}{\sum_n \int [dk_z](-\partial_\epsilon^2 f_n^0)}. \quad (A4)$$

Now, using Eqs. (A2) and (A3) in the Boltzmann equation, we obtain the nonlinear version of it as

$$-2i\omega[\delta g_n^{(21),\chi}(-\partial_\epsilon f_n^0) + \delta g_n^{(22),\chi}(-\partial_\epsilon^2 f_n^0)] - \frac{eE_z}{\hbar}\partial_{k_z}[\delta g_n^{(1),\chi}(-\partial_\epsilon f_n^0)]$$

$$= -\frac{1}{\tau}[\delta g_n^{(21),\chi} - \delta \bar{g}_n^{(21),\chi}](-\partial_\epsilon f_n^0) - \frac{1}{\tau}[\delta g_n^{(22),\chi} - \delta \bar{\bar{g}}_n^{(22),\chi}](-\partial_\epsilon^2 f_n^0) - \frac{1}{\tau_v}[\delta \bar{g}_n^{(21),\chi}(-\partial_\epsilon f_n^0) + \delta \bar{\bar{g}}_n^{(22),\chi}(-\partial_\epsilon^2 f_n^0)]. \quad (A5)$$

Now, we integrate both sides of the above equation with $\sum_n \int [dk_z]$ and divide by $\sum_n \int [dk_z](-\partial_\epsilon f_n^0)$. As the intranode scattering does not alter the number of particles within each node, all the terms $\propto 1/\tau$ on the right-hand side will get canceled. Consequently, we are left with the equation

$$
-2i\omega\delta\bar{g}_n^{(21),\chi} - 2i\omega\mathcal{D}\int_{n,k_z}\delta g_n^{(22),\chi}\left(-\partial_\epsilon^2 f_n^0\right) - eE_z\mathcal{D}\int_{n,k_z}v_{z,n}^\chi\delta g_n^{(1),\chi}\left(-\partial_\epsilon^2 f_n^0\right) - eE_z/\hbar\mathcal{D}\int_{n,k_z}\partial_{k_z}\delta g_n^{(1),\chi}\left(-\partial_\epsilon f_n^0\right)
$$

$$
= -\frac{1}{\tau_v}\delta\bar{g}_n^{(21),\chi} - \frac{1}{\tau_v}\mathcal{D}\int_{n,k_z}\delta\bar{\bar{g}}_n^{(22),\chi}\left(-\partial_\epsilon^2 f_n^0\right). \tag{A6}
$$

Here, we have defined $\sum_n \int [dk_z] \equiv \int_{n,k_z}$ and $1/\mathcal{D} \equiv \sum_n \int [dk_z](-\partial_\epsilon f_n^0)$ for brevity. Now, from our definition of $\delta\bar{g}_n^{(21),\chi}$, in the above equation we identify

$$
\delta\bar{g}_n^{(21),\chi} = \frac{e\tau_{v,2\omega}E_z/\hbar\sum_n\int[dk_z](-\partial_\epsilon f_n^0)\partial_{k_z}\delta g_n^{(1),\chi}}{\sum_n\int[dk_z](-\partial_\epsilon f_n^0)}. \tag{A7}
$$

With this, the integrated Boltzmann equation, Eq. (A6), reduces to

$$
2i\omega\int_{n,k_z}\delta g_n^{(22),\chi}\left(-\partial_\epsilon^2 f_n^0\right) + eE_z\int_{n,k_z}v_{z,n}^\chi\delta g_n^{(1),\chi}\left(-\partial_\epsilon^2 f_n^0\right)
$$

$$
= \frac{1}{\tau_v}\int_{n,k_z}\delta\bar{\bar{g}}_n^{(22),\chi}\left(-\partial_\epsilon^2 f_n^0\right). \tag{A8}
$$

Dividing the above equation by $\sum_n \int [dk_z](-\partial_\epsilon^2 f_n^0)$, we obtain the other part of the local distribution function as

$$
\delta\bar{\bar{g}}_n^{(22),\chi} = \frac{e\tau_{v,2\omega}E_z\sum_n\int[dk_z]v_{z,n}^\chi\delta g_n^{(1),\chi}\left(-\partial_\epsilon^2 f_n^0\right)}{\sum_n\int[dk_z]\left(-\partial_\epsilon^2 f_n^0\right)}. \tag{A9}
$$

Finally, we use Eqs. (A7) and (A9) in Eq. (A5) to obtain the second-order NL distribution function. The two components are calculated to be

$$
\delta g_n^{(21),\chi} = e\tau_{2\omega}E_z/\hbar\partial_{k_z}\delta g_n^{(1),\chi} + \tau_{2\omega}\frac{\kappa}{\tau_v}\delta\bar{g}_n^{(21),\chi}, \tag{A10a}
$$

$$
\delta g_n^{(22),\chi} = e\tau_{2\omega}E_z v_{z,n}^\chi\delta g_n^{(1),\chi} + \tau_{2\omega}\frac{\kappa}{\tau_v}\delta\bar{\bar{g}}_n^{(22),\chi}. \tag{A10b}
$$

Now using the NDF, we calculate the 2ω component of the longitudinal current density, defined as

$$
j_z(2\omega) = -e\mathfrak{D}\sum_{n,\chi}\int[dk_z]v_{z,n}^\chi\big[\delta g_n^{(21),\chi}\left(-\partial_\epsilon f_n^0\right)
$$

$$
+ \delta g_n^{(22),\chi}\left(-\partial_\epsilon^2 f_n^0\right)\big]. \tag{A11}
$$

After a little algebra, we find that the NL longitudinal conductivity has the following form:

$$
\sigma_{zzz}(2\omega) = -\frac{e^3\tau_\omega\tau_{2\omega}}{4\pi^2 l_B^2}\sum_\chi\Bigg[\frac{\mathfrak{I}^\chi}{\hbar^2} + \frac{\kappa}{\tau_v}\Bigg\{\frac{\mathcal{C}_{11}^\chi}{\mathcal{C}_{01}^\chi}(\tau_{v,\omega}\mathcal{C}_{22}^\chi
$$

$$
+ \tau_{v,2\omega}\mathcal{I}^\chi) + \tau_{v,2\omega}\frac{\mathcal{C}_{12}^\chi}{\mathcal{C}_{02}^\chi}\bigg(\mathcal{C}_{22}^\chi + \kappa\frac{\tau_{v,\omega}}{\tau_v}\frac{\mathcal{C}_{11}^\chi}{\mathcal{C}_{01}^\chi}\mathcal{C}_{12}^\chi\bigg)\Bigg\}\Bigg]. \tag{A12}
$$

This is the exact expression of the NL conductivity discussed in this paper. Note that $\sigma_{zzz}(2\omega)$ contains all the NL chiral anomaly coefficients defined in the main text in Eqs. (10a) and (10b). Using the results of the main text, $\mathcal{C}_{12}^\chi = 0$ and $\mathcal{C}_{22}^\chi =$

$-\mathcal{I}^\chi$, it is evident that the chiral anomaly contribution to the NL magnetoconductivity becomes identically zero in the DC limit ($\omega = 0$). Furthermore, in the case of AC transport limit, where we can consider $\omega\tau_v \ll 1$, which is the interest of this paper, we can ignore all the contributions from the internode scattering since in this limit $\tau_{v,\omega} \approx \tau_{v,2\omega}$.

APPENDIX B: CALCULATION OF LANDAU LEVELS IN MULTI-WEYL SEMIMETALS

In this Appendix, we present the details of the LL calculation of the tilted multi-WSMs [51]. For that, we write the Hamiltonian given in Eq. (20) as

$$
\mathcal{H}_\chi^\nu = \chi[\alpha_\nu\{(\hbar\hat{k}_-)^\nu\sigma_+ + (\hbar\hat{k}_+)^\nu\sigma_-\} + \hbar vk_z\sigma_z] + \hbar\boldsymbol{w}_\chi\cdot\boldsymbol{k}\sigma_0, \tag{B1}
$$

where $\hat{k}_\pm = \hat{k}_x \pm i\hat{k}_y$, $\sigma_\pm = \frac{1}{2}(\sigma_x \pm i\sigma_y)$. We choose the gauge potential to be $\boldsymbol{A} = (-By, 0, 0)$ for the magnetic field along the z direction, parallel to the tilt velocity $\boldsymbol{w}_\chi = (0, 0, w_{\|,\chi}) = v(0, 0, t_{\|,\chi})$. Consequently, the translation symmetry remains invariant along the x and z directions. Hence, we look for the solution of the form $\mathcal{H}_\chi^\nu\Psi = \epsilon_n\Psi$, where $\Psi = \psi(y)e^{i\hbar(k_x x + k_z z)}$. With such plane wave basis the Hamiltonian is modified as

$$
\mathcal{H}_\chi^\nu = \chi\begin{pmatrix} \hbar vk_z + \chi\hbar w_{\|,\chi}k_z & \alpha_\nu(\hbar k_x - eBy - i\hbar\hat{k}_y)^\nu \\ \alpha_\nu(\hbar k_x - eBy + i\hbar\hat{k}_y)^\nu & -\hbar vk_z + \chi\hbar w_{\|,\chi}k_z \end{pmatrix}. \tag{B2}
$$

To diagonalize the above Hamiltonian, we introduce a new variable $\tilde{y} = (y/l_B - k_x l_B)$, and subsequently the creation and annihilation operators $\hat{a}^\dagger = 1/\sqrt{2}(\tilde{y} - \partial_{\tilde{y}})$ and $\hat{a} = 1/\sqrt{2}(\tilde{y} + \partial_{\tilde{y}})$, satisfying the commutation relation $[\hat{a}, \hat{a}^\dagger] = 1$. Using these we obtain

$$
\mathcal{H}_\chi^\nu = \chi\begin{pmatrix} \hbar vk_z + \chi\hbar w_{\|,\chi}k_z & (-1)^\nu\omega_\nu(\hat{a})^\nu \\ (-1)^\nu\omega_\nu(\hat{a}^\dagger)^\nu & -\hbar vk_z + \chi\hbar w_{\|,\chi}k_z \end{pmatrix}, \tag{B3}
$$

with $\omega_\nu = \alpha_\nu(\sqrt{2}\hbar/l_B)^\nu$. One can obtain the LLs for the above Hamiltonian using the spinor (i) $\psi(y) = [a_\nu\psi_{n-\nu} \quad b_\nu\psi_\nu]^T$ when $n \geqslant \nu$, and (ii) $\psi(y) = [0 \quad \psi_0]^T$ when $n < \nu$. Here, ψ_ν are the usual harmonic oscillator wave functions, and a_ν and b_ν are the normalization constants. We have provided the LL spectrums in Eq. (21).

From Eq. (21), we notice that similar to the WSMs, for the multi-WSMs also the tilt introduces a constant velocity parallel to the magnetic field, which is crucial for nonzero NL response in the system. Furthermore, the topological charge of the WSMs (ν) manifests through the LL spectrum when subjected to a strong magnetic field, which in turn modifies the NL magnetoconductivity in multi-WSMs.

[1] X. Wan, A. M. Turner, A. Vishwanath, and S. Y. Savrasov, Phys. Rev. B **83**, 205101 (2011).

[2] A. A. Burkov and L. Balents, Phys. Rev. Lett. **107**, 127205 (2011).

[3] M. Z. Hasan, S.-Y. Xu, I. Belopolski, and S.-M. Huang, Annu. Rev. Condens. Matter Phys. **8**, 289 (2017).

[4] B. Yan and C. Felser, Annu. Rev. Condens. Matter Phys. **8**, 337 (2017).

[5] N. P. Armitage, E. J. Mele, and A. Vishwanath, Rev. Mod. Phys. **90**, 015001 (2018).

[6] B. Q. Lv, T. Qian, and H. Ding, Rev. Mod. Phys. **93**, 025002 (2021).

[7] H. Nielsen and M. Ninomiya, Phys. Lett. B **130**, 389 (1983).

[8] A. A. Zyuzin and A. A. Burkov, Phys. Rev. B **86**, 115133 (2012).

[9] D. T. Son and B. Z. Spivak, Phys. Rev. B **88**, 104412 (2013).

[10] H.-J. Kim, K.-S. Kim, J.-F. Wang, M. Sasaki, N. Satoh, A. Ohnishi, M. Kitaura, M. Yang, and L. Li, Phys. Rev. Lett. **111**, 246603 (2013).

[11] M.-X. Deng, G. Y. Qi, R. Ma, R. Shen, R.-Q. Wang, L. Sheng, and D. Y. Xing, Phys. Rev. Lett. **122**, 036601 (2019).

[12] K. Das and A. Agarwal, Phys. Rev. Research **2**, 013088 (2020).

[13] K. Das, S. K. Singh, and A. Agarwal, Phys. Rev. Research **2**, 033511 (2020).

[14] M. N. Chernodub, Y. Ferreiros, A. G. Grushin, K. Landsteiner, and M. A. H. Vozmediano, arXiv:2110.05471

[15] K. Das and A. Agarwal, Phys. Rev. B **103**, 125432 (2021).

[16] H. Li, H. He, H.-Z. Lu, H. Zhang, H. Liu, R. Ma, Z. Fan, S.-Q. Shen, and J. Wang, Nat. Commun. **7**, 10301 (2016).

[17] J. Xiong, S. K. Kushwaha, T. Liang, J. W. Krizan, M. Hirschberger, W. Wang, R. J. Cava, and N. P. Ong, Science **350**, 413 (2015).

[18] H. Weng, C. Fang, Z. Fang, B. A. Bernevig, and X. Dai, Phys. Rev. X **5**, 011029 (2015).

[19] B. Q. Lv, H. M. Weng, B. B. Fu, X. P. Wang, H. Miao, J. Ma, P. Richard, X. C. Huang, L. X. Zhao, G. F. Chen, Z. Fang, X. Dai, T. Qian, and H. Ding, Phys. Rev. X **5**, 031013 (2015).

[20] S.-Y. Xu, I. Belopolski, N. Alidoust, M. Neupane, G. Bian, C. Zhang, R. Sankar, G. Chang, Z. Yuan, C.-C. Lee, S.-M. Huang, H. Zheng, J. Ma, D. S. Sanchez, B. Wang, A. Bansil, F. Chou, P. P. Shibayev, H. Lin, S. Jia *et al.*, Science **349**, 613 (2015).

[21] S.-M. Huang, S.-Y. Xu, I. Belopolski, C.-C. Lee, G. Chang, B. Wang, N. Alidoust, G. Bian, M. Neupane, C. Zhang, S. Jia, A. Bansil, H. Lin, and M. Z. Hasan, Nat. Commun. **6**, 7373 (2015).

[22] A. A. Zyuzin, S. Wu, and A. A. Burkov, Phys. Rev. B **85**, 165110 (2012).

[23] G. Chang, B. Singh, S.-Y. Xu, G. Bian, S.-M. Huang, C.-H. Hsu, I. Belopolski, N. Alidoust, D. S. Sanchez, H. Zheng, H. Lu, X. Zhang, Y. Bian, T.-R. Chang, H.-T. Jeng, A. Bansil, H. Hsu, S. Jia, T. Neupert, H. Lin *et al.*, Phys. Rev. B **97**, 041104(R) (2018).

[24] H.-Y. Yang, B. Singh, J. Gaudet, B. Lu, C.-Y. Huang, W.-C. Chiu, S.-M. Huang, B. Wang, F. Bahrami, B. Xu, J. Franklin, I. Sochnikov, D. E. Graf, G. Xu, Y. Zhao, C. M. Hoffman, H. Lin, D. H. Torchinsky, C. L. Broholm, A. Bansil *et al.*, Phys. Rev. B **103**, 115143 (2021).

[25] R. Boyd, *Nonlinear Optics* (Academic Press, San Diego, CA, 2008).

[26] L. Wu, S. Patankar, T. Morimoto, N. L. Nair, E. Thewalt, A. Little, J. G. Analytis, J. E. Moore, and J. Orenstein, Nat. Phys. **13**, 350 (2017).

[27] Q. Ma, S.-Y. Xu, C.-K. Chan, C.-L. Zhang, G. Chang, Y. Lin, W. Xie, T. Palacios, H. Lin, S. Jia, P. A. Lee, P. Jarillo-Herrero, and N. Gedik, Nat. Phys. **13**, 842 (2017).

[28] C.-K. Chan, N. H. Lindner, G. Refael, and P. A. Lee, Phys. Rev. B **95**, 041104(R) (2017).

[29] E. J. König, H.-Y. Xie, D. A. Pesin, and A. Levchenko, Phys. Rev. B **96**, 075123 (2017).

[30] L. E. Golub, E. L. Ivchenko, and B. Z. Spivak, JETP Lett. **105**, 782 (2017).

[31] B. Sadhukhan and T. Nag, Phys. Rev. B **103**, 144308 (2021).

[32] B. Sadhukhan and T. Nag, Phys. Rev. B **104**, 245122 (2021).

[33] F. de Juan, A. G. Grushin, T. Morimoto, and J. E. Moore, Nat. Commun. **8**, 15995 (2017).

[34] X. Yang, K. Burch, and Y. Ran, arXiv:1712.09363.

[35] Z. Li, Y.-Q. Jin, T. Tohyama, T. Iitaka, J.-X. Zhang, and H. Su, Phys. Rev. B **97**, 085201 (2018).

[36] Y. Gao and B. Ge, Opt. Express **29**, 6903 (2021).

[37] F. de Juan, Y. Zhang, T. Morimoto, Y. Sun, J. E. Moore, and A. G. Grushin, Phys. Rev. Research **2**, 012017(R) (2020).

[38] I. Sodemann and L. Fu, Phys. Rev. Lett. **115**, 216806 (2015).

[39] H. Rostami and M. Polini, Phys. Rev. B **97**, 195151 (2018).

[40] Y. Gao, F. Zhang, and W. Zhang, Phys. Rev. B **102**, 245116 (2020).

[41] T. Morimoto, S. Zhong, J. Orenstein, and J. E. Moore, Phys. Rev. B **94**, 245121 (2016).

[42] A. A. Zyuzin, M. Silaev, and V. A. Zyuzin, Phys. Rev. B **98**, 205149 (2018).

[43] V. A. Zyuzin, Phys. Rev. B **98**, 165205 (2018).

[44] R.-H. Li, O. G. Heinonen, A. A. Burkov, and Steven S.-L. Zhang, Phys. Rev. B **103**, 045105 (2021).

[45] C. Zeng, S. Nandy, and S. Tewari, Phys. Rev. B **105**, 125131 (2022).

[46] T. Nag and D. M. Kennes, arXiv:2201.11417.

[47] D. E. Kharzeev, Y. Kikuchi, R. Meyer, and Y. Tanizaki, Phys. Rev. B **98**, 014305 (2018).

[48] L. E. Golub and E. L. Ivchenko, Phys. Rev. B **98**, 075305 (2018).

[49] Y. Gao and F. Zhang, Phys. Rev. B **103**, L041301 (2021).

[50] X. Li, B. Roy, and S. Das Sarma, Phys. Rev. B **94**, 195144 (2016).

[51] A. Gupta, Phys. Lett. A **383**, 2339 (2019).

[52] R. M. A. Dantas, F. Peña-Benitez, B. Roy, and P. Surówka, J. High Energy Phys. 12 (2018) 069.

[53] A. Menon, S. Chattopadhay, and B. Basu, Phys. Rev. B **104**, 075129 (2021).

[54] S. P. Mukherjee and J. P. Carbotte, Phys. Rev. B **97**, 045150 (2018).

[55] S. Nandy, C. Zeng, and S. Tewari, Phys. Rev. B **104**, 205124 (2021).

[56] T. Nag and S. Nandy, J. Phys.: Condens. Matter **33**, 075504 (2021).

[57] L. X. Fu and C. M. Wang, Phys. Rev. B **105**, 035201 (2022).

[58] F. Xiong, C. Honerkamp, D. M. Kennes, and T. Nag, arXiv:2202.08610.

[59] A. Menon and B. Basu, J. Phys.: Cond. Matter **33**, 045602 (2020).

[60] T. Nag, A. Menon, and B. Basu, Phys. Rev. B **102**, 014307 (2020).

[61] K. Sonowal, A. Singh, and A. Agarwal, Phys. Rev. B **100**, 085436 (2019).

[62] K. Das and A. Agarwal, Phys. Rev. B **99**, 085405 (2019).

[63] K. Das and A. Agarwal, Phys. Rev. B **100**, 085406 (2019).

[64] Z.-M. Yu, Y. Yao, and S. A. Yang, Phys. Rev. Lett. **117**, 077202 (2016).

[65] Q. Chen, A. R. Kutayiah, I. Oladyshkin, M. Tokman, and A. Belyanin, Phys. Rev. B **99**, 075137 (2019).

[66] J. Shao and L. Yan, J. Phys.: Condens. Matter **33**, 185704 (2021).

[67] M. O. Goerbig, J.-N. Fuchs, G. Montambaux, and F. Piéchon, Europhys. Lett. **85**, 57005 (2009).

[68] J. Sári, M. O. Goerbig, and C. Tőke, Phys. Rev. B **92**, 035306 (2015).

[69] V. Lukose, R. Shankar, and G. Baskaran, Phys. Rev. Lett. **98**, 116802 (2007).

[70] S. Vadnais and R. Côté, Phys. Rev. B **104**, 144409 (2021).

[71] K. Landsteiner, Acta Phys. Pol., B **47**, 2617 (2016).

[72] M.-X. Deng, H.-J. Duan, W. Luo, W. Y. Deng, R.-Q. Wang, and L. Sheng, Phys. Rev. B **99**, 165146 (2019).

[73] V. A. Zyuzin, Phys. Rev. B **95**, 245128 (2017).

[74] P. Bhalla, K. Das, D. Culcer, and A. Agarwal, arXiv:2108.04082.

[75] S. Lahiri, T. Bhore, K. Das, and A. Agarwal, Phys. Rev. B **105**, 045421 (2022).

[76] C. Zeng, S. Nandy, P. Liu, S. Tewari, and Y. Yao, arXiv:2203.01196.